This full text paper was peer-reviewed at the direction of IEEE Instrumentation and Measurement Society prior to the acceptance and publication.

Thermal and RGB-D Imaging for Necrotizing Enterocolitis Detection

Yangyu Shi[1], Pierre Payeur[1], Monique Frize[2] and Erika Bariciak[3]

[1]School of Electrical Engineering and Computer Science, University of Ottawa, Canada
[2]Department of Systems and Computer Engineering, Carleton University, Canada
[3]Department of Pediatrics, Children's Hospital of Eastern Ontario, Canada

***Abstract*—Necrotizing enterocolitis (NEC) is a severe condition in neonates, typically involving inflammation in the small intestine. In this paper, a novel automated image acquisition and analysis system combining an infrared thermal camera with a RGB-D sensor is proposed for detection of NEC in preterm newborns. Calibration procedures are defined to ensure frame synchronization and observation consistency among the color, depth and infrared images. Segmentation and extraction of the body are automatically performed on the infrared image with the help of the additional color and depth information collected by the RGB-D sensor. Automated analysis of the temperature distribution over the entire abdominal region minimizes interference from manual intervention and facilitates operation in a clinical environment. An experimental comparison of temperature distribution in normal babies and those with NEC demonstrates encouraging initial results.**

Keywords—NEC detection, infrared thermal imaging, RGB-D sensing, thermal distribution analysis, image processing.

I. INTRODUCTION

Neonatal necrotizing enterocolitis (NEC) is an acquired disease, usually seen in preterm infants, with non-specific symptoms such as abdominal distension, blood in the stool, and feeding intolerance as the main clinical manifestations [1]. The morbidity and mortality of NEC are significant and decrease with increasing gestational age and weight, and are higher for babies who require surgery for treatment [2, 3]. The etiology of NEC is not well understood and the lack of specific clinical manifestations makes early clinical diagnosis of NEC difficult. Radiographic imaging of the abdomen is currently the preferred diagnostic method in a clinical environment. Although x-ray examinations have great value in the mid- and late-stage diagnosis of NEC, early x-ray examinations are still non-specific, expose the baby to ionizing radiation, and require handling of these very sick patients [4].

Infrared thermal (IR) imaging is an advanced functional medical imaging detection technology, which uses a thermal imaging camera to receive different levels of infrared radiation from different parts of the human body and converts them into temperature values for disease diagnosis and human functional status evaluation. Because it only passively receives thermal radiation generated by the metabolism of human cells, it does not require contact with the body, does not emit radiation, and thus does not cause any damage or side effects to the human body. The most prominent role of infrared thermal imaging in medical detection is early warning of physical disorders. In the early stages of many diseases, only functional (metabolic) changes appear instead of organic lesions, which means that the temperature changes precede lesions, and functional changes precede pathological changes [5]. While radiographic imaging can be effective only after the disease has developed, medical infrared thermal imaging collects information on temperature changes, which can reveal hidden dangers without any obvious symptoms, and can detect problems earlier.

Rice et al. [6, 7] compared the temperature distribution of certain abdominal segments to that of the chest and found that IR imaging can accurately detect temperature differences over the anatomical area. Herry et al. [8] applied IR imaging to the field of NEC diagnosis by comparing abdominal thermal images of normal premature infants with those of infants diagnosed with NEC. Experiments showed that the rate of change in the abdominal surface temperature of the two groups was significantly different. Like in previous studies, Ntonfo et al. [9] selected a rectangular region on the abdominal temperature map. They then retrieved thermal features represented by sample distributions from values of the 8-bit grayscale palette to perform the analysis. Frize et al. [10] found that the temperature distribution on the upper-to-lower (UL) region of the abdomen showed a difference sufficient to distinguish infants with and without NEC.

Although prior studies have provided valuable insights, they are also limited by various sources of bias or interference. First, the position of the IR camera was not standardized in all of the previous studies, which could result in differences in the ability to extract the affected abdominal regions and the ability to directly compare images. Second, manual selection of regions of interest for temperature distribution analysis was used, which increases the possibility of biased results and limits its accessibility as a bedside tool. Therefore, the purpose of this study was to develop a more standardized, easy-to-use and data-driven diagnostic assistance tool which could be used for NEC detection. The paper presents an automated IR thermal imaging and analysis approach guided by an RGB-D sensor to improve the accessibility and reliability of the IR imaging procedure.

978-1-7281-5386-5/20/$31.00 ©2020 IEEE

II. METHODOLOGY

The automated multispectral acquisition and analysis system combines a Microsoft Kinect Xbox One sensor and a FLIR Thermovision A320 IR camera. Both devices work together to synchronously capture color, depth, and IR images in real-time. The system processes the color and depth images to segment areas of interest on the human body from the background. The segments are mapped to the IR images automatically to extract the relevant thermal distribution information that is finally analyzed.

Fig. 1 presents a flow chart of the proposed approach, which is made up of three main components: design of the acquisition platform and its calibration, segmentation and feature extraction from multispectral images, and analysis of the thermal distribution within regions of interest in the IR images. In the first component, the Kinect sensor is used to collect color and depth images, which are aligned to form RGB-D images based on the parameters of the sensor itself. The FLIR IR camera is used to acquire IR images of the whole body. Then the RGB-D and IR images are inter-calibrated to match corresponding pixels in images from the different sensors. In the second part, image segmentation procedures are performed with the help of depth and RGB color information to remove the background, refine the definition of the body area, identify specific body parts, and extract the abdominal area as the region of interest. The extracted segment is mapped to the calibrated IR image to retrieve the thermal distribution over the abdomen. Afterwards, pixel values related to temperature are processed into thermal signatures that are analyzed with classical first-order statistical measures, which allows for comparison and analysis between different groups of preterm infants.

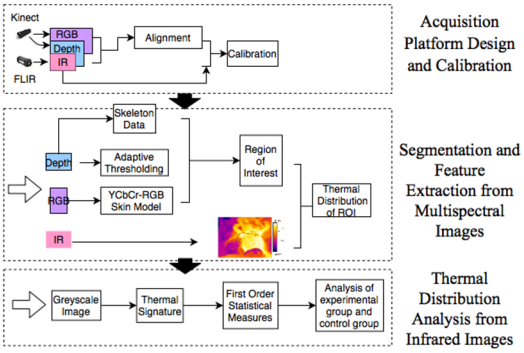

Fig. 1. Flow chart of the automated multispectral acquisition and analysis system.

A. Design of the Image Acquisition System

The Kinect Xbox One sensor, shown in Fig. 2a, consists of one RGB camera that collects 1920 x 1080 color images, and one depth sensor that records the depth information in 512 x 424 format with an average depth accuracy of 0.002 - 0.004m. The OpenNI2 driver is used to access to the Kinect sensor by initializing the device and receiving original image streams. The FLIR A320 IR camera, shown in Fig. 2b, collects 320 x 240 thermal images with an accuracy of ±3.6°F. The Atlas SDK for .NET developed by FLIR is used to control the IR camera.

Both devices are mounted on a rigid stand, with wheels for moving flexibly in a clinical environment, as shown in Fig. 2c. The camera assembly is designed to be positioned above the subject who lies on a bed surface, therefore imaging along a close to vertical optical axis and producing images of the baby from above, as depicted in Fig. 3a. Considering that the IR camera has a narrower field of view than the Kinect sensor, the former is positioned further away from the subject, thereby minimizing the gap between the surfaces imaged by the two devices. A distance of about 20 cm was experimentally determined to be appropriate. The Kinect sensor is assembled about 12 cm aside from the IR camera to prevent occluding part of the subject, as shown in Fig. 2d. Meanwhile, the imaging planes and optical axes of the two sensors need to remain parallel without tilting. The sensor assembly is designed with a 15-degree inclination to facilitate full-body imaging of the baby from the bedside. Finally, since the Kinect sensor emits in a spectral range of 827 - 850 nm, while the IR camera is sensitive in the spectrum range from 7.5 to 13 μm, the two sensors do not interfere with each other.

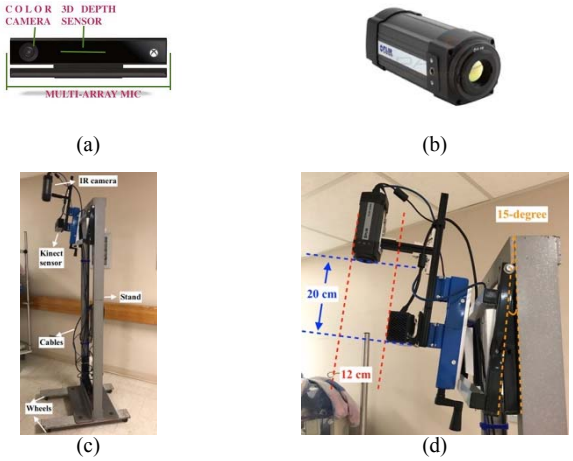

(a) (b) (c) (d)

Fig. 2. Image acquisition system devices and assembly: (a) Kinect Xbox One sensor; (b) FLIR A320 IR camera; (c) assembly of the imaging device; (d) close up view of assembly on Kinect sensor and IR camera.

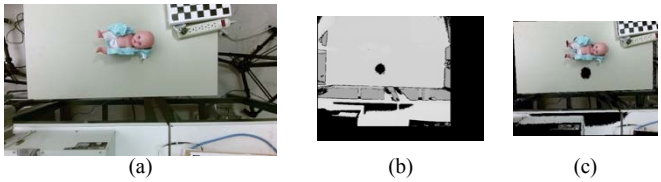

(a) (b) (c)

Fig. 3. RGB-D image reconstruction: (a) original color image; (b) original depth image; (c) RGB-D image.

B. Calibration

The calibration procedure begins with registering the color and depth images to form an RGB-D image. The coordinate mapping class in OpenNI2 is used to align the depth and RGB images, where color pixels are matched with the corresponding pixels in the depth map when the depth pixel is valid. If the pixel in the depth map is invalid, then the corresponding pixel in the RGB-D image will be black, as displayed by black holes in Fig. 3b and 3c.

Zhang's classical checkerboard calibration method was adopted for inter-calibration between the RGB-D and IR sensors [11]. For that purpose, a custom checkboard was designed for feature detection, as shown in Fig. 4. The checkboard is made up of a 13 x 9 grid of black and white squares with a size of 28mm that are sharply detected by the Kinect sensor. Furthermore, 49 incandescent light bulbs are embedded at every second corner of the grid to emit heat, which can be detected as hot spot features by the IR camera.

(a) (b)

Fig. 4. Custom multispectral calibration checkerboard made up of 13 x 9 black and white squares with 49 embedded incandescent light bulbs at intersection points: a) color image of calibration board under normal ambient lighting conditions, and b) IR image of calibration board with incandescent bulbs forming hot spots.

Fig. 4b shows a typical IR image of the custom calibration board, where the brighter (red) areas indicate the positions of the higher-temperature incandescent bulbs, while the darker (blue) areas represent the relatively low temperature background. In order to input valid feature points from the hot spots that match with the black and white checkerboard pattern into the calibration tool, pre-processing is performed as follows:

1) Apply gray-level thresholding to the original IR image (Fig. 5a);

2) Perform erosion operation to eliminate noise and connect adjacent elements within the whole image (Fig. 5b);

3) Detect lines of hot spots using Hough Transform [12] (Fig. 5c) and divide lines into two perpendicular groups, represented in solid and dotted lines in Fig. 5d. The rotation angle for each group is determined as the mean angle from all lines in the group;

4) For each line in the solid group, locate its intersection with all lines in the dotted group. As shown in Fig. 5e, it results in 49 feature points corresponding to the 49 embedded lights;

5) In order to match with all feature points in the RGB-D image, fill the remaining feature points of the checkerboard by estimating the midpoints of any two adjacent hot spots to complete the set of features in the IR image (Fig. 5f).

Afterwards, stereo calibration is performed in between the IR camera and RGB-D sensor after acquiring multiple checkerboard images from various angles with both devices. The GML Calibration Toolbox [13] is used to calculate the intrinsic and extrinsic parameters. As seen from Fig. 6 and Table 1, with respect to the IR camera, the Kinect depth camera in the assembly is estimated at -117± 7mm aside in the horizontal direction, X, 189 ± 16mm away in the vertical direction, Z, and deviates from the center of the IR camera by 15 ± 2mm, Y. These experimental calibration results are coherent with the set relative distances of about -12cm and 20cm defined in section II.A, and with the inherent distance of the RGB camera from the Kinect sensor's center. Rotation estimates are small, meaning the two sensors have close to parallel optical axes, which does not impede on the multi-modal imaging process.

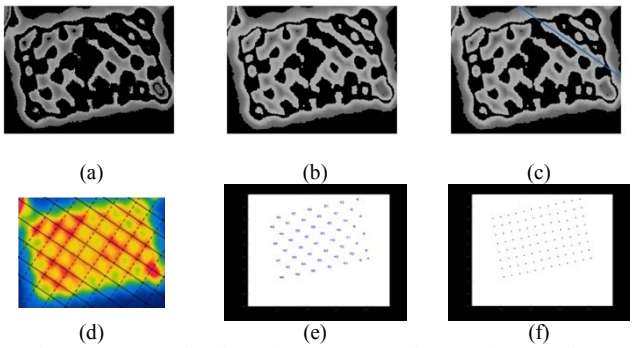

(a) (b) (c)

(d) (e) (f)

Fig. 5. Pre-processing the IR image to extract hot spot feature points.

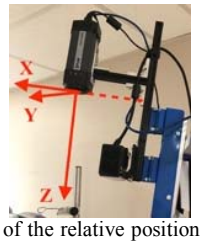

Fig. 6. Coordinates system of the relative position of the RGB-D sensor with respect to the IR camera.

Table 1. Extrinsic parameters (Kinect depth sensor wrt IR camera).

Rotation	R = [-0.11806 0.09681 0.00154] ± [0.00729 0.00818 0.00015] rad
Translation	T = [-117.23159 14.68501 188.79907] ± [6.67013 2.11307 16.07277] mm

C. *Segmentation*

Since the color and depth data contain valuable information to help retrieve the structure of the human body, they are effectively used to subdivide the IR image in different parts that would otherwise adversely influence the detection of NEC due to a similar temperature distribution. Thus, a segmentation method based on the three sets of calibrated images is introduced, first relying on the depth information to extract regions of interest and then on the color information to refine the human body area, before thermal maps extracted only from relevant parts of the IR image are closely analyzed to help with the diagnosis.

First, a dynamic depth threshold is applied to isolate the body from the flat bedding surface. Based on the histogram of the depth map, the distance threshold is determined automatically by the first significant observed cluster according to the imaging conditions defined above that involve imaging the subject from above. The selected cluster is shown by the red box in Fig. 7a. A first approximate segment containing the baby's body is obtained as seen in Fig. 7b.

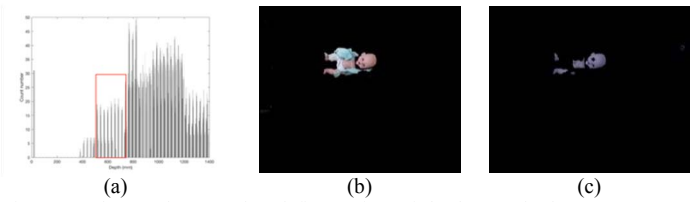

(a) (b) (c)

Fig. 7. Background removal and fine-tuning of the human body segments: (a) histogram of Fig. 3b; (b) background removal with dynamic depth threshold; and (c) RGB-D segmentation refinement with skin color filter.

Second, a skin color model coded in the YCbCr space is used to refine the segmentation of exposed body regions from other objects in the field of view, such as probes, tubes, or clothes, as shown as Fig. 7c.

Third, a skeleton recognition method based on the depth image is introduced as an additional refinement step, where depth data is utilized to recognize some skeleton points and describe different parts of the human body. The method includes the following steps:

1) Traverse the pre-segmented RGB-D image after skin filter application (Fig. 8a) from its four edges to find the closet circular segment, considered as the head of the baby, using Halcon template matching function [14] (Fig. 8b);

2) Detect all contours with Canny edge detection (Fig. 8c);

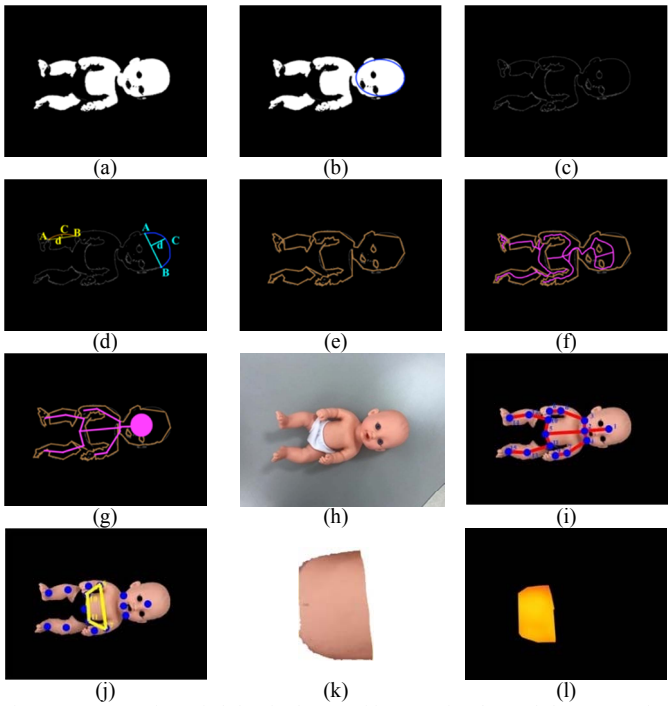

Fig. 8. Segmentation of abdominal area of interest for thermal data extraction performed over a mock baby doll: (a) depth image after background removal and fine-tuning of the human body region; (b) closest circular part, considered as the baby's head within blue circle; (c) Canny edges detection; (d) polygonal approximation algorithm; (e) discretized external contour curve into an external polygon; (f) skeleton points based on local distance maxima algorithm; (g) skeleton lines in the largest connected domain with other branches removed; (h) color image of the baby doll; (i) complete skeleton data and joint points distribution with order numbers; (j) initial definition of the abdominal region; (k) final segmentation of abdominal region of interest; and (l) corresponding region of interest on the thermal map to be analyzed.

3) Discretize the external contour curve into an external polygon using a polygonal approximation algorithm, which consists of the following steps:

a) For each fragment of contour, connect between two points A, B, at the beginning and end of one curve, as shown in Fig. 8d;

b) Obtain point C which has the largest distance away from AB;

c) Compare the distance with a predetermined threshold range. If it is within the range, then AB is used as an approximation of the curve; if it is smaller, then ignore it;

d) If the distance is larger than the range, such as the right line in Fig. 8d, then subdivide curve segment and perform steps (a)-(c) on AC and CB, respectively;

e) Fig. 8e shows the external polygon after all curves are processed.

4) Select a point p within the external polygon and two points q_1, q_2 on the external polygon closest to p (with q_1, q_2 on different sides) to determine the local maximum Euclidean distance for the skeleton location. Based on the work of Hesse et al. [15], if p is the local maximum, then p is the skeleton point. Fig. 8f shows the initial skeleton structure;

5) Take the head part determined in step 1 as one skeleton point and optimize the rest of skeleton lines with the polygonal approximation algorithm described in step 3 (Fig. 8g);

6) Consider the endpoints of each bone line as joint points. As demonstrated on an image of a mock baby (Fig. 8h), each joint point is numbered starting from the head, following the next unlabeled joint point adjacent to the current joint point. For multiple joint points adjacent to the current skeleton point, the joint point above or to the left takes precedence, and the other direction has lower priority (Fig. 8i);

7) Define the initial abdominal region of interest as an area surrounded by the four feature points 6, 7, 10, 11, as marked in yellow in Fig. 8j;

8) Refine the region of interest toward the actual abdominal region for thermal data extraction with the skin color filter described above. The final segmentation result is shown in Fig. 8k.

Fourth, the segmented abdominal region of interest is mapped from the RGB-D image onto the calibrated IR image while taking into account the different resolution of images. The calibration board mentioned in section II.B is used to measure the ratio of the length of the blocks in the RGB-D and the IR maps. All sets of RGB-D and IR images acquired simultaneously are used to estimate the scaling parameters and the mapping coefficient is determined by averaging the estimates. The thermal map segment corresponding to the abdominal region of interest depicted in Fig. 8k is shown in Fig. 8l.

D. Thermal Distribution Analysis

Once the abdominal region of interest is automatically defined and the corresponding region of the IR thermal image is extracted, the temperature values distribution within the entire area of interest is analyzed. All values considered for analysis are grayscale levels in the IR image rather than absolute temperature. First-order statistics are computed on the distribution and box plots are prepared to closely examine the distributions and compare temperature differences between different groups of subjects [9].

III. EXPERIMENTAL VALIDATION

After obtaining ethics approval, a total of 10 normal babies and 2 babies diagnosed with NEC were recruited and imaged at

the bedside in a neonatal intensive care unit (NICU), following strict approved protocols. The normal babies were between 29+0 - 41+0 weeks corrected gestational age without any clinical or radiological signs commonly associated with NEC. The NEC cases had typical signs and symptoms of NEC and xray images that corresponded to definitive NEC (Bell's stage 2) [4]. To ensure confidentiality, baby's images are blurred.

As shown in Fig. 9, the sensors assembly was placed at bedside with the two sensors oriented vertically down toward the subject, and the distance between the sensor and the subject was about 60 cm. The whole data acquisition process took less than two minutes; the bed heat source was turned off for 60 sec to allow for skin surface cooling and to ensure that only infrared radiation emitted by the baby is recorded. Then imaging was performed for approximately 60 seconds.

Fig. 9. Data collection at NICU.

An example of image processing results is presented in Fig. 10 for a normal subject. An original RGB-D image is shown in Fig. 10a, with the results of background removal with depth thresholding (Fig. 10b) and skin color filter (Fig. 10c). The proposed skeleton recognition approach was applied to estimate logical joint points over the body (Fig. 10d), which were then used to define the initial abdominal area of interest for thermal data analysis, as marked with the blue quadrilateral in Fig. 10e. In this example, although the two legs were not recognized since they were separated from the torso in the images by the diaper worn by the subject, the four feature points used to define the initial abdominal region (Fig. 10f) were not affected. The skin color filter was applied again to refine the accuracy of the region of interest segment, as shown in Fig. 10g, leading to the extraction of thermal data (Fig. 10h) over only the corresponding abdominal area in Fig. 10i.

The thermal data of 10 normal babies and 2 babies with NEC were analyzed using first-order statistics after converting data to grayscale levels. By observing the raw data of the normal group and the NEC group individually, it was observed that the heat distribution characteristics of the samples within each group are similar. Moreover, the first-order statistics and box plot diagrams are basically less sensitive to the size of the data. Therefore, in order to make the data of the normal and NEC groups clearer, data of each group was combined to obtain the overall normal and NEC groups' heat distributions. Results are reported in Table 2 and Fig. 11a, with units corresponding to grayscale levels in the IR image associated with temperature.

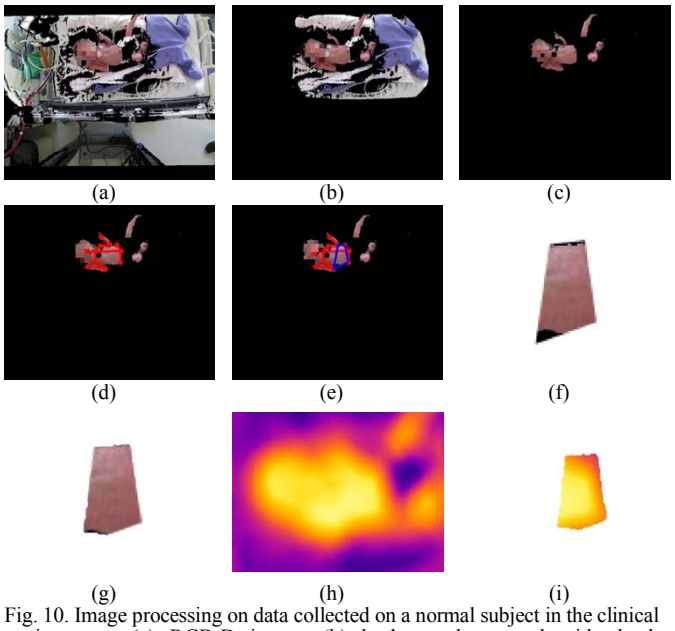

Fig. 10. Image processing on data collected on a normal subject in the clinical environment: (a) RGB-D image; (b) background removal with depth threshold; and (c) with skin color filter; (d) detected skeleton joint points; (e) initial abdominal area; (f) refined close-up view of initial abdominal region; (g) refined abdominal region of interest; (h) IR thermal image; and (i) corresponding abdominal segment from IR thermal image.

Table 2. Statistical measures over 2 NEC and 10 normal subjects with the proposed method and with comparative method.

	NEC (proposed)	**Normal (proposed)**	**NEC (comparative) [9]**	**Normal (comparative) [9]**
Mean	161	129	151	132
Median	180	153	180	161
Standard variance	39	50	55	51
Min	26	1	1	1
Max	195	175	195	175
Skewness	-1.29	-0.78	-1.3	-0.98
Median absolute deviation	31.8	44.0	44.9	44.2
Interquar-tile range	52	86	69	75
Kurtosis	3.54	2.23	3.53	2.69

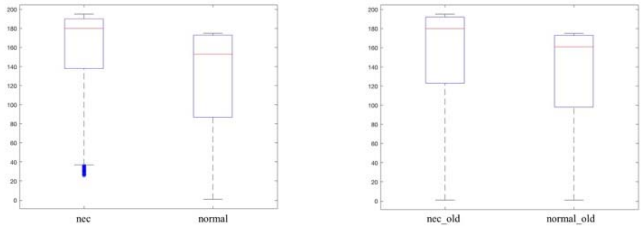

(a) (b)

Fig. 11. Box plot of NECs and normals: a) proposed approach; and b) comparative method [9].

Using the proposed method, the mean and median of grayscale values for the normal group are lower than that of the NEC group, suggesting that intestinal inflammation affecting the NEC babies triggers a rise in the abdominal temperature. In

addition, the box plot of the NEC group is shorter than that of the normal one, showing that the data are more concentrated in general. Also, the median line of the NEC group is closer to the upper quartile, revealing that the temperature data are distributed on the right side of the X-axis and the data are more left-biased than that of the normal group.

Results are compared with those obtained on the same dataset of infants with and without NEC, but using image analysis methods that manually select a rectangular region of interest over the abdominal area, as proposed in [9]. As seen in the two last columns of Table 2 and Fig. 11b, the mean and median temperatures still show differences between the normal and NEC groups. However, using this manual image processing approach we observe less significant differences in the thermal distribution between the two groups. The box plots from the two methods show that the dispersion of the two groups is more similar, and that both groups are left-biased at a similar degree.

Further comparison with the raw statistical values reported in [9] also reveals some discrepancies in the distribution of the mean thermal values for NEC (146) and normal (166) subjects in comparison with values reported in Table 2. The variability is related to: *i)* different dataset sizes (2 subjects in [9] versus 12 in this work); *ii)* babies recruited in each study were at different stages of NEC; and *iii)* acquisition of data was performed with different IR thermal cameras with different resolutions and temperature to grayscale mapping.

In order to derive strong conclusions on thermal distribution trends for NEC versus normal subjects, further experimental evaluation on larger number of samples, and use of a unique IR camera, will be necessary. The proposed method contributes to a more uniform procedure for data acquisition and thermal values extraction over a more comprehensive surface of the abdominal area of interest, while reducing influence from manual intervention in the procedure.

IV. CONCLUSION AND DISCUSSION

This paper provides unique insights on the use of IR imaging technology in combination with an RGB-D sensor, to augment the detection of newborns affected by intestinal inflammatory disorders such as NEC. The assembly of multi-modal sensors and corresponding calibration procedures improve the uniformity of thermal data extraction that is critical for reliable comparative temperature distribution analysis upon which diagnosis assistance relies. Color and depth information is fully utilized to automate and refine segmentation results compared to traditional standalone IR image processing that involves substantial manual intervention by trained medical personnel. The temperature distribution analysis over the entire abdominal area ensures that all available and relevant information is taken advantage of while minimizing external interference.

Our early experimental results on data acquired from newborn babies in the clinical environment demonstrated an increase in the abdominal temperature distribution in babies diagnosed with NEC, which could be explained by heat generated by inflammation associated with NEC. Temperature variation was also observed in previous work [9], however the differences in temperature distribution between the two groups may be related to the small sample size, different acquisition protocols and IR camera resolution, and different data processing procedures used in this comparative study.

Our study demonstrates emerging validity of the proposed acquisition and analysis framework. Future work will involve thermal data analysis on a larger set of NEC cases, and comprehensive analysis of the normal and NEC groups using more advanced data distribution analysis methods.

ACKNOWLEDGMENTS

The authors acknowledge support from Natural Sciences and Engineering Research Council of Canada.

REFERENCES

[1] Neu, J & Walker, A. (2011). Necrotizing Enterocolitis. *New England Journal of Medicine*, 364: 255-64.

[2] Niemarkt, H. J., de Meij, T. G., van de Velde, M. E., van der Schee, M. P., Van Goudoever, J. B., Kramer, B. W., Andriessen, P., & de Boer, N. K. (2014). Necrotizing enterocolitis: a clinical review on diagnostic biomarkers and the role of the intestinal microbiota. *Inflammatory Bowel Diseases*, 21(2), 436-444.

[3] Neu, J. (2015). Preterm infant nutrition, gut bacteria, and necrotizing enterocolitis. *Current Opinion in Clinical Nutrition and Metabolic Care*, 18(3), 285.

[4] Bell, M. J., Ternberg, J. L., Feigin, R. D., Keating, J. P., Marshall, R., Barton, L., & Brotherton, T. (1978). Neonatal necrotizing enterocolitis. Therapeutic decisions based upon clinical staging. *Annals of Surgery*, 187(1), 1.

[5] Nur, R., & Frize, M. (2013). Image processing of infrared thermal images for the detection of necrotizing enterocolitis. In *Medical Imaging: Image Processing* ,Vol. 8669. International Society for Optics and Photonics.

[6] Rice, H. E., Hollingsworth, C. L., Bradsher, E., Danko, M. E., Crosby, S. M., Goldberg, R. N., Tanaka, D.T., & Knobel, R. B. (2010). Infrared thermal imaging (thermography) of the abdomen in extremely low birthweight infants. *Journal of Surgical Radiology*, 1(2), 61-122.

[7] Knobel, R. B., Guenther, B. D., & Rice, H. E. (2011). Thermoregulation and thermography in neonatal physiology and disease. *Biological Research for Nursing*, 13(3), 274-282.

[8] Herry, C. L., Frize, M., & Bariciak, E. (2011). Assessment of abdominal skin temperature change in premature newborns with NEC compared to healthy controls. In *5th European Conference of the International Federation for Medical and Biological Engineering*, pp. 191-194. Springer, Berlin, Heidelberg.

[9] Ntonfo, G. K., Frize, M., & Bariciak, E. (2015). Detection of Necrotizing Enterocolitis in newborns using abdominal thermal signature analysis. In *Proceedings of the IEEE International Symposium on Medical Measurements and Applications (MeMeA)*, pp. 36-39.

[10] Frize, M., Nur, R., Bariciak, E., & Herry, C. (2013). Infrared Imaging and Classification of Neonates with Necrotising Enterocolitis. In *World Congress on Medical Physics and Biomedical Engineering*, May 26-31, 2012, Beijing, China, pp. 1309-1312. Springer, Berlin, Heidelberg.

[11] Zhang, Z. (2000). A flexible new technique for camera calibration. *IEEE Transactions on Pattern Analysis and Machine Intelligence*, 22.

[12] Duda, R. O., & Hart, P. E. (1971). Use of the Hough transformation to detect lines and curves in pictures (No. SRI-TN-36). Sri International Menlo Park Ca Artificial Intelligence Center.

[13] Graphics and Media Lab, GML C++ Camera Calibration Toolbox. Accessed on: Sep 10, 2018. Avaible: http://graphics.cs.msu.ru/en/node/909.

[14] "Summary of template matching method based on Halcon". Aug 1, 2018. Access on: Jan 22, 2020. [Online]. Available: https://topic.alibabacloud.com/a/summary-of-template-matching-method-based-on-halcon_8_8_10275122.html.

[15] Hesse, N., Stachowiak, G., Breuer, T., Arens, M. (2015), "Estimating Body Pose of Infants in Depth Images Using Random Ferns". *Proc. of the IEEE Intl Conf. on Computer Vision Workshops*, pp. 35-43.